Stability of Fe-based alloys with structure type C_6Cr_{23}

M. Widom and M. Mihalkovič*

Department of Physics

Carnegie Mellon University

Pittsburgh, PA 15213

(Dated: July 28, 2004)

Bulk metallic glass forms when liquid metal alloys solidify without crystalization. In the search for Iron-based bulk glass-forming alloys of the metal-metalloid type (Fe-B- and Fe-C-based), crystals based on the structural prototype C_6Cr_{23} often preempt the amorphous phase. Destabilizing this competing crystal structure could enhance glass-formability. We carry out first-principles total energy calculations of enthalpy of formation to identify third elements that can effectively destabilize C_6Cr_{23}. Yttrium appears optimal among transition metals, and rare earths also are suitable. Atomic size is the dominant factor.

PACS numbers: 61.50.Lt,61.43.Dq, 71.20.Be, 81.30.Bx

I. INTRODUCTION

Iron-based amorphous alloys are used in transformer cores, where their low magnetic coercivity reduces energy loss. Popular glass-forming alloys are based on Fe together with metalloid elements such as B or C. Bulk Iron-based amorphous alloys could become important structural materials, but optimal glass-forming compositions are not yet known. Multicomponent alloys containing fourth row transition metals and rare earths show promise [1–3].

We previously explored the quaternary B-Fe-Y-Zr phase diagram [4], identifying stable and metastable crystal phases and computing their enthalpies of formation. This study identified crystalline structures based on the C_6Cr_{23} prototype as important competitors to glass formation. It appeared that the competition is more problematic in the case of B-Fe-Zr than in the case of B-Fe-Y. To ensure the optimal selection of alloy system, we now carry out a systematic study of many candidate "third elements" and compare them with regard to stability of the C_6Cr_{23} structure. We do this both for the case of B-Fe- and C-Fe-based alloys. We show that atomic size mismatch

---

*Also at Institute of Physics, Slovak Academy of Sciences, 84228 Bratislava, Slovakia

destabilizes the C_6Cr_{23} structure for sufficiently large atoms such as Yttrium and rare earths [2, 5, 6].

II. METHODS

Our *ab-initio* calculations use the program VASP [7, 8] together with the projector-augmented wave method, an all-electron generalization of the pseudopotential approach [9, 10]. We employ the Perdew-Wang generalized gradient approximation [11] (GGA) exchange-correlation functional with the Vosko-Wilkes Nussair [12] spin interpolation. These choices give excellent results for bulk elemental Fe [10]. GGA is needed instead of LDA is necessary to properly reproduce magnetization and lattice constants [13]. Our magnetic calculations are spin-polarized (i.e. collinear magnetization) and are employed for any structure containing 50% Fe or higher. All calculations for Carbon-based binaries and ternaries are performed at a constant cutoff energy of 400 eV, the default for our Carbon potential. All calculations for Boron-based binaries and ternaries are performed at 320 eV, the default for our Boron potential. More details and discussion of convergence, etc. are given in Ref. [4]. All the ab-initio data on which this paper is based can be obtained on the WWW at Ref. [14].

The composition space of an N-component alloy is a set of N composition variables forming an $N-1$ dimensional simplex (respectively, a point, line segment, triangle and tetrahedron for $N = 1, 2, 3, 4$). Structural energies form a scatter-plot over this simplex. Stable low temperature phases lie on vertices of this scatter-plot. Edges and facets of the convex hull represent coexistence regions of the phases at adjoining vertices.

The tie-lines and tie-planes connecting all pure elements in their lowest energy structures forms a useful reference for alloy energies. The distance ΔH_{for} of an alloy energy from the tie-surface joining pure elements is known as its enthalpy of formation. It is an enthalpy because volume relaxation means we work at fixed pressure, $P = 0$. Strong compound formation is reflected in large negative enthalpy of formation. The value of ΔH is determined solely by the cohesive energy of a given structure relative to the cohesive energies of its constituent pure elements.

High temperature phases should lie above the convex hull, but be sufficiently close that entropic effects (e.g. atomic vibrations, vacancies or chemical substitution) can stabilize them. Metastable phases also should lie close to the convex hull, so that their free energy is less than the liquid free energy at temperatures below freezing. Although ΔH_{for} is usually negative for high temperature and metastable phases, their energy difference ΔE from the convex hull is small and positive. ΔE measures the thermodynamic driving force for decomposition into the appropriate combination of stable phases. In contrast to ΔH, the value of ΔE depends on the cohesive energies of other competing structures. Discovery of a new stable structure will increase the assessed ΔE values of previously known structures.

In principle all possible combinations and arrangements of atoms should be considered to ensure the optimal possibilities are found. This is clearly impossible. Rather, we choose plausible structures for consideration by chemical substitution into known structures of similar compounds [15]. We especially consider alloy systems with similar atomic size ratios or other chemical properties.

Structures are denoted using their prototype names and Pearson symbols. For example, we will be interested in the C_6Cr_{23} prototype. The element Cr will be replaced by Fe, and in some cases the element C will be replaced by B. The Pearson symbol for the C_6Cr_{23} prototype is cF116, indicating cubic symmetry, face-centering, with 116 atoms per unit cell. The *primitive* cell of C_6Cr_{23}.cF116 contains 116/4=29=23+6 atoms.

Using these methods, we built a database of structural energies. For a given N-component alloy system of interest we extract from our database energies of structures containing all, of just some, of the chosen elements. We use a standard convex hull program (qhull [16]) to identify stable structures and the coexistence regions that connect them. Based on the output of this program, we calculate values of ΔH_{for} and ΔE for every structure. Numerical data for the compounds considered here, and more than 1500 others, can be found at Ref. [14].

III. RESULTS

A. Binaries

Cohesive energies of binary B-Fe and C-Fe alloys are shown in Fig. 1. Our results for both alloy systems are in perfect qualitative agreement with experiment [17, 18], because all the known low temperature stable phases occur on the convex hulls (notice C-Fe has no stable compounds) and all the know high temperature, metastable and unknown hypothetical structures lie above the hull. It is impressive how sensitive the density functional theory is to differences in chemical identity, with the many distinctions between B-Fe and C-Fe all being faithfully reproduced.

Many metastable phases are known in the C-Fe binary system. Two of these, CFe_4.cP5 and CFe_3.hP8 are based on FCC Iron with Carbon interstitials in, respectively, tetrahedral and octahedral sites. The CFe_3.oP16 structure is also an important metstable phase in B-Fe. It can be considered as a strong distortion of the Fe_3Si.cF16 structure, caused by the small atomic sizes of B and C relative to Si. Similarly, the energies of the interstitial cP5 and hP8 structures are lower for C than for B because the Carbon atoms are smaller than Boron. The chief B-Fe structures are discussed further in Ref. [4].

The lowest-lying metastable C-Fe binary compound has the structure of C_6Cr_{23}. This crystal structure appears to

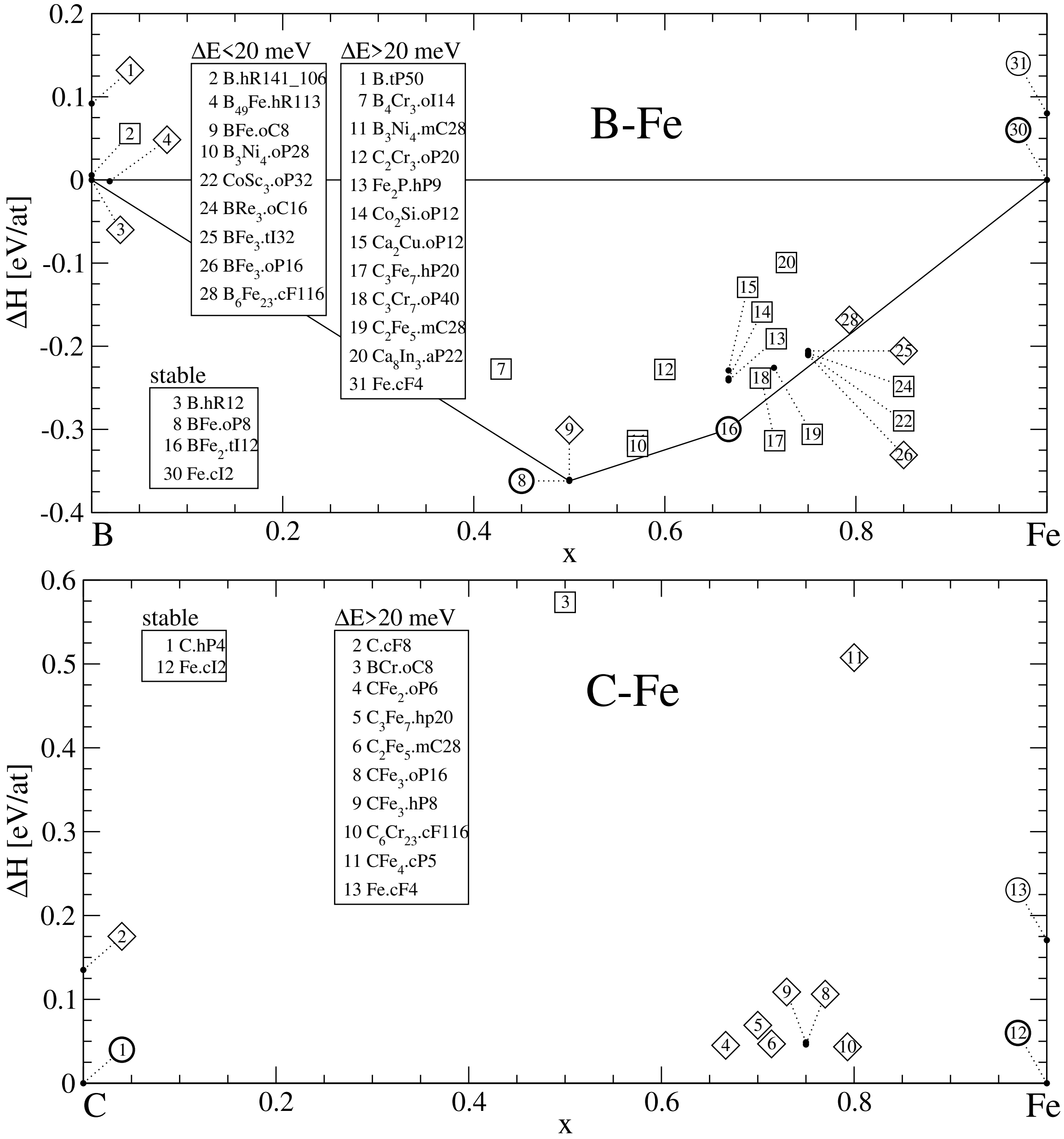

FIG. 1: Enthalpies of formation and their convex hulls for the B-Fe (top) and C-Fe (bottom) binary alloys. Notation: heavy circles denote known low temperature phases, light circles denote known high temperature phases, diamonds denote known metastable phases, squares denote unreported structures.

be the most important competitor to metallic glass formation, and further destabilizing it is the goal of this work.

To evaluate stabilities of a ternary alloy system such as C-Fe-Y we need to examine all three of its binary subsystems. The Fe-Y diagram was previously discussed in [4] and need not be repeated here. The C-Y binary phase diagram is poorly known [19, 20], with three phases (β-$C_{19}Y_{15}$ and α,β-C_3Y_2) of unknown structure. The reported stable low temperature tP68 structure of α-$C_{19}Y_{15}$ (isostructural with $C_{19}Sc_{15}$.tP68) suffers from large displacements during

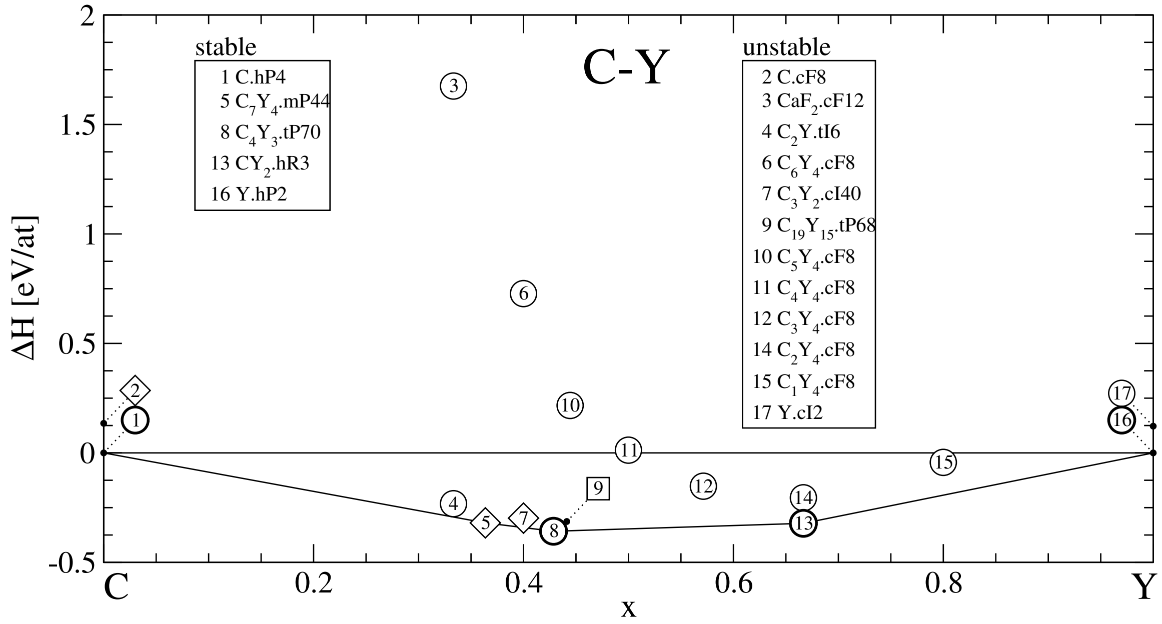

FIG. 2: Enthalpies of formation and their convex hull for the C-Y binary alloys. Notation as in Fig. 1

relaxation, and a final relaxed energy above the convex hull. We find instead that C_4Y_3.tP70 [15] is stable at low temperatures.

The high temperature γ phase probably takes the reported Fe_4N.cF8 structure in the Y-rich limit. This structure is based upon an FCC lattice of Y atoms with C occupying octahedral interstitial sites. When these sites are fully occupied the unit cell composition is C_4Y_4 and the structure becomes NaCl. On the C-rich side, we begin occupying tetrahedral interstitials and the energy rapidly grows beyond values that are plausible for a high temperature phase. We also tested Y vacancies and found them even higher in energy. We believe the γ phase actually terminates at 50% Carbon, rather than the reported 67%. The postulated β-C_2Y.cF12 structure [19] at 67% Carbon (based on an FCC lattice of Y with C fully occupying all tetrahedral interstitials) is highly unstable and presumably incorrect.

B. Ternaries

Having verified the ability to reproduce these binary phase diagrams, we now investigate ternary systems. Fig 3 illustrates a typical ternary energy diagram, in this case for the alloy C-Fe-Y. This diagram confirms stability of previously known ternary phases and also proposes B_2Fe_2Y.tI10 as stable, though this structure has not previously been reported [21]. We also propose C_2FeSc.tP8 as the probable structure of a previously reported metastable phase of unknown structure. Similar energy diagrams for all ternaries discussed below may be found at Ref. [14].

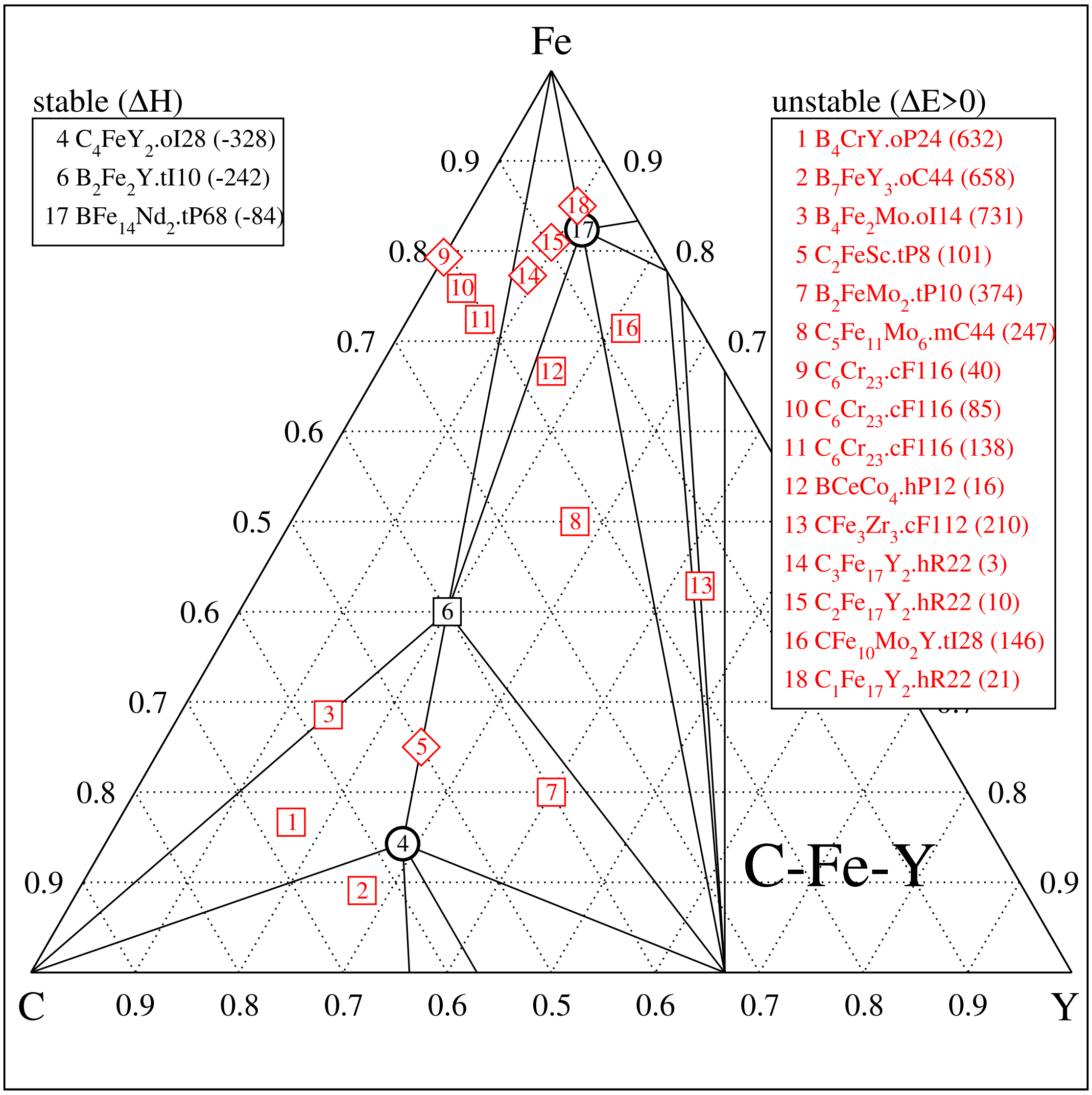

FIG. 3: Energy diagram for ternary C-Fe-Y. Plotting symbols as in Fig. 1. Values in parenthesis indicate enthalpy of formation ΔH_{for} for stable compounds, and energies above the convex hull ΔE for metastable structures.

We now focus our attention on one specific structure, C_6Cr_{23}, and examine its stability for a variety of B-Fe- and C-Fe-based ternaries. Although Chromium-based in the prototype structure, it is a well known metastable phase in Iron-based alloys such as C-Fe-Mo and we predict it is actually stable in B-Fe-Sc, B-Fe-Nb and B-Fe-Mo.

Our plan is to find elements that can mix with the binaries in the liquid state but that will destabilize C_6Cr_{23} due to their large atomic size. The requirement of miscibility in the liquid state rules out alkali metals and alkali earths. The requirement of large atomic size rules out middle and late transition metals. We thus identify the primary candidates as the early transition metals and the rare earths.

TABLE I: Site energies (ΔE (eV/atom)), near-neighbor distances and Voronoi volumes for Y substitution on different Wyckoff classes.

site	4a	8c	32f	48h
energy	0.135	0.085	0.145	0.146
r_Y	2.62	2.71	2.42	2.40
V	20.1	24.5	23.7	22.4

Our discussion begins with Yttrium, the first transition metal of row 4 in the periodic table. The first question to address is the optimal site for Y atoms. As a large atom, it cannot enter as an interstitial, nor can it substitute for Carbon. There are thus 4 plausible sites, the Iron sites of Wyckoff classes 4a, 8c, 32f or 48h (see Table I).

Table I evaluates the relaxed energies of a single 29 atom primitive cell of cF116 with one Y atom replacing one Fe atom, respectively, on each distinct Fe site. Evidently Y atoms favor Wyckoff class 8c, most likely as a result of their large size. Indeed, placing Y on site 8c results in both the largest Voronoi volume V for Y atoms and the largest near-neighbor distance r_Y.

We also checked that the 8c site is prefered for a *second* Y substitution, after the first Y atom is already on 8c. Since there are only two 8c sites in a primitive cell (8/4=2) this corresponds to complete filling of the 8c sites with Y atoms. Double occupancy of the 8c site by the large atom is consistent with the solved crystallographic structure of $B_6Co_{21}Zr_2$, which is isostructural with C_6Cr_{23}.

The following energy study focuses on the case of double substitution to fully occupy the 8c sites. The energy cost for occupying both 8c sites by Y is more than twice the cost for occupying just one, as can be seen by comparing tables I and II. The energies for 0, 1 and 2 Y-atom substitutions on site 8c in C6Fe23 are, respectively, ΔE=0.043, 0.085 and 0.141 eV/atom in a 29 atom primitive cell. So the first substitution costs $29 \times (0.085 - 0.043) = 1.22$ eV, while the second costs $29 \times (0.141 - 0.085) = 1.62$ eV. Presumably this is because lattice strains created by insertion of the first Y atom are accomodated partly by shrinkage of the volume around the second 8c position. When the second Y atom is introduced this accomodation is no longer possible.

A picture of the cF116 structure at composition $C_6Fe_{21}Y_2$ is shown in Fig. 4. The 8c sites have coordination number $Z = 16$, with only Fe atom neighbors. The Voronoi polyhedron (Watson and Bennett [22] class (0,0,12,4)) has 12 pentagonal faces and 4 hexagonal faces, characteristic of local tetrahedral close packing. The Voronoi polyhedron is illustrated in Fig. 4. However, the remainder of the structure does not exhibit tetrahedral packing.

The Carbon sites, Wyckoff class 24e, have a Voronoi polyhedron (Watson and Bennett class (0,8,0)) with 8 square

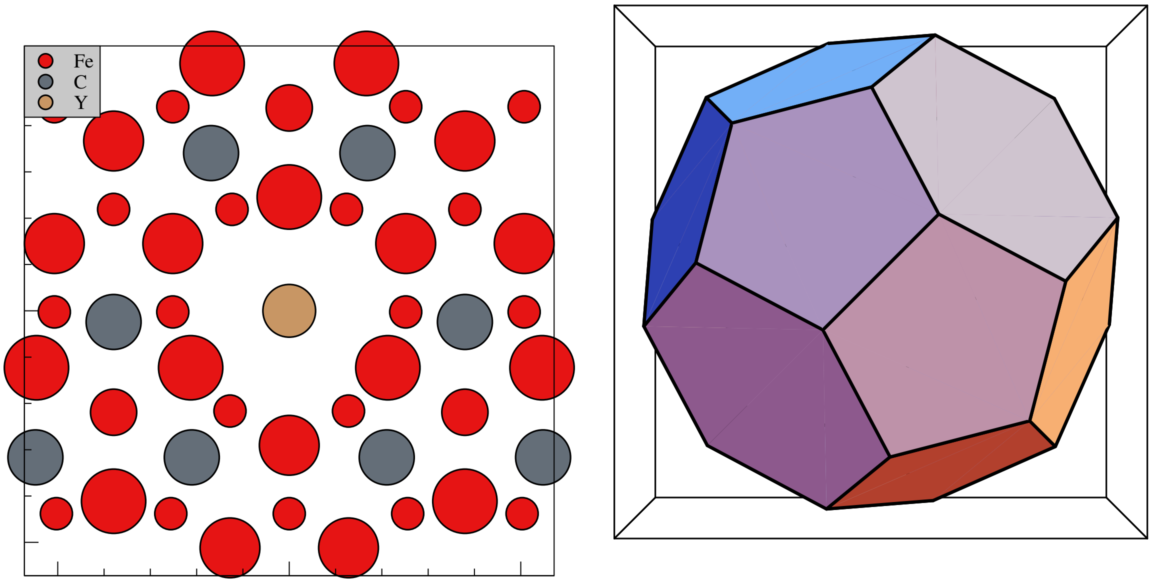

FIG. 4: (left) Structure of C6Fe21Y2.cF116 viewed along (1,1,1). Atom size indicates height. Hash marks are 1 Å. (right) Voronoi polyhedron of Y site, Wyckoff class 8c, viewed along (1,0,0).

faces and a highly nongeneric four-fold vertex. The eight neighbors of each Carbon atom are Iron atoms at distances of 2.05 and 2.15 Å, substantially greater than the 1.79-1.99 Å found in other metastable C-Fe structures. This loose binding of the Carbon atom probably explains why the C_6Cr_{23} structure is actually more favorable for B-Fe than for C-Fe, because Boron is slightly larger.

Now we compare the stabilities with different choices of large atom. Our data is presented in Table II for several choices of large atom. In each case we verified that the 8c site is prefered. We fully occupy the 8c site, with two large atoms per face-centered primitive cell. Values of r_T are distances from large atom to nearest neighbor transition metal in the fully relaxed structure.

Evidently, of the 4d transition metals, the largest atom, Yttrium, is the most effective at destabilizing C_6Cr_{23}. Indeed, Zr, Nb and Mo tend to *stabilize* it relative to the B-Fe and C-Fe binaries. However, too large a Y concentration is dangerous for glass formation, because of the low-energy metastable $C_3Fe_{17}Y_2$.hR22 structure (Y content 9.1%) and the stable structure $CFe_{14}Y_2$.tP68 (Y content 11.8%) visible in Fig. 3.

We can also test whether the 4d row is an optimal choice by examining other members of group IIIA (the first column of transition metals, consisting of Sc, Y, La and Ac). Clearly the 3d element Sc is too small to destabilize C_6Cr_{23}. Lanthanum (5d) and Actinium (6d) are both highly effective. The lanthanide and actinide rare earth elements, which behave chemically like Lanthanum and Actinium, should likewise do well. Of course, Actinides may present other

TABLE II: Energies for complete TM substitution on site 8c. the top row are B-Fe and C-Fe binaries for comparison.

^{Z}Ch	B-Fe			C-Fe		
	ΔE	ΔH	r_T	ΔE	ΔH	r_T
^{26}Fe	0.018	-0.168	2.40	0.043	0.043	2.42
^{39}Y	0.074	-0.163	2.61	0.141	0.059	2.61
^{40}Zr	0.016	-0.253	2.54	0.025	-0.037	2.54
^{41}Nb	stable	-0.246	2.48	0.002	-0.028	2.48
^{42}Mo	stable	-0.212	2.42	0.030	0.022	2.41
^{21}Sc	stable	-0.244	2.53	0.054	-0.035	2.53
^{57}La	0.094	-0.092	2.60	0.195	0.189	2.61
^{89}Ac	0.232	0.046	2.66	0.228	0.228	2.65

difficulties not considered here!

IV. CONCLUSIONS

We compared the effectiveness of different large-atom substitution as a way to destabilize the C_6Cr_{23} structure of B-Fe and C-Fe. The first task was to identify the most energetically favorable substitution site for the large atom. We found, in every case considered that Wyckoff site 8c (a locally tetrahedrally close-packed site) was most favorable. We showed that among the 4d transition metals Yttrium was the only element capable of destabilizing the C_6Cr_{23} structure relative to the binary alloy. Comparing group IIIA elements, we found that Sc was inadequate but Y, La and Ac are fine.

Clearly atomic size is a crucial consideration for destabilizing this structure. Indeed, the 8c site prefers atoms slightly larger than Fe, so replacement with Mo, Nb or Sc can actually *stabilize* cF116. We conclude that Yttrium and rare earth elements can enhance glass formation. However, too large an Yttrium concentration (9% or more) can lead to formation of other competing crystal phases such as $C_3Fe_{17}Y_2$.hR22 or $BFe_{14}Nd_2$.tP68. Alkali earth elements such as Ca are also highly effective at destabilizing C_6Cr_{23}, but they do not mix well with Fe-based alloys, at least at atmospheric pressure.

Acknowledgments

We wish to acknowledge useful discussions with Yang Wang, Don Nicholson, Joe Poon and Gary Shiflet. This work was supported by DARPA/ONR Grant N00014-01-1-0961. Portions of the calculations were performed at the Pittsburgh Supercomputer Center.

[1] Z. P. Lu, C. T. Liu, J. R. Thompson, and W. D. Porter, Phys. Rev. Lett. **92**, 245503 (2004).

[2] V. Ponnambalam, S. J. Poon, and G. J. Shiflet, J. Mat. Resch. **19**, 1320 (2004).

[3] V. Ponnambalam, S. J. Poon, G. J. Shiflet, V. M. Keppens, R. Taylor, and G. Petculescu, Appl. Phys. Lett. **83**, 1131 (2003).

[4] M. Mihalkovič and M. Widom, Phys. Rev. B (2004), submitted, cond-mat/0405298.

[5] T. Egami and Y. Waseda, J. Non-Cryst. Solids **64**, 113 (1984).

[6] D. B. Miracle and O. N. Senkov, Mat. Sci. Eng. A **347**, 50 (2003).

[7] G. Kresse and J. Furthmuller, Phys. Rev. B **54**, 11169 (1996).

[8] G. Kresse and J. Hafner, Phys. Rev. B **47**, RC558 (1993).

[9] P. Blochl, Phys. Rev. B **50**, 17953 (1994).

[10] G. Kresse and D. Joubert, Phys. Rev. B **59**, 1758 (1999).

[11] J. P. Perdew and Y. Wang, Phys. Rev. B **45**, 13244 (1992).

[12] S. H. Vosko, L. Wilk, and M. Nusair, Can. J. Phys. **58**, 1200 (1980).

[13] E. . Moroni, G. Kresse, J. Hafner, and J. Furthmuller, Phys. Rev. B **56**, 15629 (1997).

[14] Structure and energy data is available on the WWW at http://alloy.phys.cmu.edu.

[15] P. Villars, *Pearson's Handbook, Desk Edition* (ASM International, Materials Park, Ohio, 1997).

[16] C. B. Barber, D. P. Dobkin, and H. T. Huhdanpaa, ACM Trans. Math. Software **22**, 469 (1996), see web site http://www.qhull.org.

[17] T. B. Massalski et al., eds., *Binary Alloy Phase Diagrams* (ASM International, Materials Park, Ohio, 1990).

[18] H. Okamoto, ed., *Desk Handbook: Phase Diagrams for Binary Alloys* (ASM International, Materials Park, Ohio, 2000).

[19] K. A. Gschneidner and F. W. Calderwood, Bull. Alloy Phase Diagrams **7**, 564 (1986).

[20] H. Okamoto, J. Phase Equil. **17**, 548 (1996).

[21] P. Villars, A. Prince, and H. Okamoto, *Handbook of ternary alloy phase diagrams* (ASM International, Materials Park, Ohio, 1995).

[22] R. E. Watson and L. H. Bennett, Phys. Rev. B **43**, 11642 (1991).